Available online at www.sciencedirect.com
SCIENCE DIRECT
Trans. Nonferrous Met. Soc. China 16(2006) 760−765
Transactions of Nonferrous Metals Society of China
www.csu.edu.cn/ysxb/

# Parameters affecting microsegregation in phase-field simulation

ZHU Chang-sheng(朱昌盛)[1,2], WANG Zhi-ping(王智平)[2], JING Tao(荆 涛)[3], XIAO Rong-zhen(肖荣振)[2]

1. CAD Center, Lanzhou University of Technology, Lanzhou 730050, China;
2. State Key Laboratory of Gansu New Non-Ferrous Metal Materials, Lanzhou 730050, China;
3. Department of Mechanical Engineering, Tsinghua University, Beijing 10084, China

Received 9 August 2005; accepted 25 April 2006

**Abstract:** The influence of various material and computational parameters such as interface kinetic coefficient($\beta$), surface energy($\sigma$), anisotropy parameter($\gamma$) and the noise amplitude($\alpha$) upon microsegregation patterns during the crystal growth was investigated by using the phase-field model which incorporated the concentration field equations. The computed results indicate that, when the appropriate value is assigned to $\alpha$, the fluctuant scope of solute composition in the solid is steady, and the influence of $\alpha$ on microsegregation is small; the larger the interface kinetic coefficient $\beta$, the more acutely the solute composition in the solid fluctuates, but the severity of microsegregation in the front interface reduces; with the increment of anisotropy parameter $\gamma$, the fluctuation of solute composition in the solid becomes more acutely, and the severity of microsegregation in the front interface aggravates; the larger surface energy $\sigma$, the smaller the fluctuant scope of solute composition in the solid is, and the smaller the degree of microsegregation is.

**Key words:** microsegregation; phase-field approach; microstructure; numerical simulation

## 1 Introduction

Dendrites are intricate patterns that make up the microstructure of many important commercial alloys[1]. A complex shape due to the emission of secondary branches behind the growing tips of primary branches has developed[1]. Generally, it is difficult to get a perfect equilibrium situation during the solidification of alloys, because the segregation by non-equilibrium solidification always occurs except for a few cases[2]. Micro-segregation resulting from the solute redistribution causes non-equilibrium second phase, porosity and crack formation which could degrade the mechanical properties of metal products. Thus, the quantitative prediction is indeed very necessary. Experimental methods and analytic methods have even been used to predict the degree of microsegregation. But it is very difficult to observe and determine the solute segregation that appears in the small dendrite region. Moreover, the analytic models have so many assumptions that they cannot describe the actual phenomenon exactly. If it is possible to estimate the degree of microsegregation by means of computer simulation, it will be possible to predict the mechanical and physical properties of metal products.

Recently, phase-field method is very powerful in simulation of dendritic growth, and it is becoming one of the important ways to achieve the industrial prediction of the solidification microstructure[3−6]. In this paper, a phase-field model for simulation of Al-Cu binary alloys solidification was investigated, some key problems in modeling and numerical computation of this kind of advanced microstructure simulation method were solved, and the phase-field parameters such as noise amplitude, interface kinetic coefficient, anisotropy parameter and surface energy was discussed.

## 2 Mathematical model and numerical issues

To a system of an initially undercooled binary alloy of components A(solvent) and B(solute), the entropy of the system is written as[7]

$$S=\int_{\Omega}\left[s(\Phi,x,e)-\frac{1}{2}\varepsilon^2(\nabla\Phi)^2+\frac{1}{2}\delta^2(\nabla x)^2\right]\mathrm{d}\Omega \qquad (1)$$

where $s(\Phi, x, e)$ is the thermodynamic entropy density, $\Phi$ is the phase-field variable, $x$ is the mole fraction of

**Foundation item:** Project(50005011) supported by the National Natural Science Foundation of China; Project(2003AA4Z1070) supported by the National High-Tech Research and Development Program of China
**Corresponding author:** ZHU Chang-sheng; Tel: +86-931-2976093; E-mail: zhucs@lut.cn

solute B in solvent A, $e$ is the internal energy density, $\varepsilon$ and $\delta$ are coefficients which account for the phase-field and concentration gradient term corrections respectively, $\Omega$ is the region occupied by the system.

The form for the evolution of phase-field is

$$\dot{\Phi} = M_{\Phi}\frac{\delta S}{\delta \Phi} \tag{2}$$

Conservation laws govern the solute and energy density transport:

$$\frac{\mathrm{d}x}{\mathrm{d}t} = -\nabla \cdot M_x \nabla \frac{\delta S}{\delta x} \tag{3}$$

$$\frac{\mathrm{d}e}{\mathrm{d}t} = -\nabla \cdot M_e \nabla \frac{\delta S}{\delta e} \tag{4}$$

where $M_{\Phi}$, $M_x$ and $M_e$ are positive constants.

In the above equations, the variational derivatives are given by

$$\frac{\delta S}{\delta \Phi} = \frac{\partial s}{\partial \Phi} + \nabla \cdot \varepsilon^2 \nabla \Phi \tag{5}$$

$$\frac{\delta S}{\delta e} = \frac{\partial s}{\partial e} = \frac{1}{T} \tag{6}$$

$$\frac{\delta S}{\delta c} = \frac{\partial s}{\partial x} + \delta^2 \nabla^2 x = \frac{\mu_{\mathrm{A}} - \mu_{\mathrm{B}}}{T} + \delta^2 \nabla^2 x \tag{7}$$

where $\mu_{\mathrm{A}}$ and $\mu_{\mathrm{B}}$ are the chemical potentials of the solvent and solute, for and ideal solution, $\mu_{\mathrm{A}}$ and $\mu_{\mathrm{B}}$ are given by

$$\mu_{\mathrm{A}} = f_{\mathrm{A}}(\Phi, T) + \frac{RT}{v_{\mathrm{m}}}\ln(1-x) \tag{8}$$

$$\mu_{\mathrm{B}} = f_{\mathrm{B}}(\Phi, T) + \frac{RT}{v_{\mathrm{m}}}\ln(x) \tag{9}$$

The free energy of the system is given by

$$f(\Phi, x, T) = (1-x)f_{\mathrm{A}} + xf_{\mathrm{B}} + \frac{RT}{V_{\mathrm{m}}}\ln(1-x) + \ln x \tag{10}$$

where $V_{\mathrm{m}}$ is the molar volume, $R$ is the ideal gas constant, $f_{\mathrm{A}}$ and $f_{\mathrm{B}}$ are respectively the free energy densities of the pure element A and B. $f_{\mathrm{A}}$ can be written as

$$f_{\mathrm{A}} = TG_{\mathrm{A}}(\Phi) + \left[e_{s,\mathrm{A}}(T_{\mathrm{m,A}}) - C_{\mathrm{A}}T_{\mathrm{m,A}} + h(\Phi)L_{\mathrm{A}}\right]\cdot \left(1 - \frac{T}{T_{\mathrm{m,A}}}\right) - C_{\mathrm{A}}T\ln\left(\frac{T}{T_{\mathrm{m,A}}}\right) \tag{11}$$

where $C_{\mathrm{A}}$ is the specific heat, $L_{\mathrm{A}}$ is the latent heat per unit volume, the function $G_{\mathrm{A}}(\Phi)$ is given by

$$G_{\mathrm{A}}(\Phi) = W_{\mathrm{A}}\Phi^2(1-\Phi)^2 \tag{12}$$

Choosing $p(\Phi)=\Phi^3(10-15\Phi+6\Phi^2)$ indicates that the bulk solid and liquid are described by $\Phi=0$ and $\Phi=1$. The free energy $f_{\mathrm{B}}$ is given by an expression similar to Eqn.(11), with the material parameters labeled with the superscript A replaced with the ones related to the B species.

Using the thermodynamic equation:

$$\frac{\partial s}{\partial \Phi} = -\frac{1}{T}\frac{\partial f}{\partial \Phi} \tag{13}$$

the governing equations of the evolution of phase-field, concentration and thermal field are written as

$$\frac{\partial \Phi}{\partial t} = M_{\Phi}\left(\varepsilon^2\nabla^2\Phi - (1-x)H_{\mathrm{A}}(\Phi, T) - xH_{\mathrm{B}}(\Phi, T)\right) \tag{14}$$

where the function $H_{\mathrm{A}}(\Phi, T)$ is defined as

$$H_{\mathrm{A}}(\Phi, T) = G'(\Phi) - p'(\Phi)L_{\mathrm{A}}\frac{T - T_{\mathrm{m,A}}}{TT_{\mathrm{m,A}}} \tag{15}$$

The dynamic equation for the concentration field is written as

$$\frac{\partial x}{\partial t} = -\nabla \cdot \left\{ D_x x(1-x)\frac{v_{\mathrm{m}}}{R}\nabla\left(\delta^2\nabla^2 x\right) - D_x\nabla x + \nabla \cdot D_x x(1-x)\frac{v_{\mathrm{m}}}{R}\left[H_{\mathrm{A}}(\Phi, T) - H_{\mathrm{B}}(\Phi, T)\right]\right\} \tag{16}$$

where

$$D_x = D_{\mathrm{s}} + p(\Phi)(D_{\mathrm{l}} - D_{\mathrm{s}}) \tag{17}$$

$D_{\mathrm{l}}$ and $D_{\mathrm{s}}$ are the diffusivities in the liquid and solid, respectively.

The equal solid and liquid thermal conductivities $K$ are assumed. $M_{\Phi}$, $W$ and $\varepsilon$ are the phase-field parameters which are related to the physical parameters as shown in the following:

$$M_{\mathrm{A}} = \frac{(T_{\mathrm{m,A}})^2\beta_{\mathrm{A}}}{6\sqrt{2}L_{\mathrm{A}}\delta_{\mathrm{A}}}, \quad M_{\mathrm{B}} = \frac{(T_{\mathrm{m,B}})^2\beta_{\mathrm{B}}}{6\sqrt{2}L_{\mathrm{B}}\delta_{\mathrm{B}}} \tag{18}$$

$$W_{\mathrm{A}} = \frac{3\sigma_{\mathrm{A}}}{\sqrt{2}T_{\mathrm{m,A}}\delta_{\mathrm{A}}}, \quad W_{\mathrm{B}} = \frac{3\sigma_{\mathrm{B}}}{\sqrt{2}T_{\mathrm{m,B}}\delta_{\mathrm{B}}} \tag{19}$$

$$\varepsilon^2 = \frac{6\sqrt{2}\sigma_{\mathrm{A}}\delta_{\mathrm{A}}}{T_{\mathrm{m,A}}} = \frac{6\sqrt{2}\sigma_{\mathrm{B}}\delta_{\mathrm{B}}}{T_{\mathrm{m,B}}} \tag{20}$$

where $\sigma$ is the interfacial energy, $\beta$ is the kinetic coefficient, $T_{\mathrm{m,A}}$ and $T_{\mathrm{m,B}}$ are the melting points of pure materials A and B, $L_{\mathrm{A}}$ and $L_{\mathrm{B}}$ are the latent heat of pure materials A and B, and $\delta_{\mathrm{A}}$ and $\delta_{\mathrm{B}}$ are the interface thickness of pure materials A and B.

For simplicity, the approximations are made that $x_{\mathrm{A}}=x_{\mathrm{B}}$, $W_{\mathrm{A}}=W_{\mathrm{B}}=W$.

For an initial nucleus of the radius $r_0$,

When $X^2+Y^2 \leqslant r^2$,

$\phi=1$, $T=T_0$, $x=x_0$ (21)

When $X^2+Y^2>r^2$,

$\phi=-1$, $T=T_0$, $x=x_0$ (22)

where $X$ and $Y$ are the coordinate axes, $T_0$ is the initial temperature of the undercooled melt, and $x_0$ is the initial alloy composition, $x_0$=0. 491 1.

The Zero-Neumann boundary conditions for $\Phi$ and $x$ are imposed at the boundaries of the computational domain[8]. The constant temperature condition was used that the boundary temperature was fixed at 1 543 K.

The noise was included as proposed in Ref.[8] by modifying the phase-field equation:

$$\dot{\Phi} \to \dot{\Phi} - M_{\Phi}\alpha r(16g(\Phi))((1-x)H_A + xH_B) \quad (23)$$

where $r$ is a random number distributed uniformly between −1 and +1, a new number is generated for every point of the grid, at each time-step, $\alpha$ is an amplitude of the fluctuations taken as 0.4.

The Ni-Cu alloy was selected. The physical properties for Ni-Cu alloy used in calculation are shown in Table 1.

**Table 1** Material parameters for Ni-Cu Alloy

| Parameters | $T_m$/ K | $L$/ (J·cm$^{-3}$) | $v_m$/ (cm$^3$·mol$^{-1}$)1) | $\beta$/ (cm·ks$^{-1}$)2) |
|---|---|---|---|---|
| Nickel(A) | 1 728 | 2 350 | 7.0 | 0.33 |
| Copper(B) | 1 358 | 1 728 | 7.8 | 0.36 |
| Parameters | $\sigma$/ (J·cm$^{-2}$) | $K$/ (cm$^2$·s$^{-1}$) | $D_l$/ (cm$^2$·s$^{-1}$) | $D_s$/ (cm$^2$·s$^{-1}$) |
| Nickel(A) | $3.75\times10^{-5}$ | 0.155 | $10^{-5}$ | $10^{-9}$ |
| Copper(B) | $2.8\times10^{-5}$ | 0.155 | $10^{-5}$ | $10^{-9}$ |

1) An average value of Ni and Cu will be taken;
2) From the data of CONTI et al[8].

## 3 Results and discussion

### 3.1 Dendrite pattern and concentration field

Fig.1 show the dendrite pattern and concentration field in the undercooled Ni-Cu alloy melt respectively. From the figures, it can be seen that the concentration profiles agree well with the dendrite pattern. And Fig.1(b) clearly shows the solute segregation both in solid and liquid phases. The concentration in the primary arm's spine, as well as in the secondary arm's spine is relatively low, because the curvature undercooling is aroused by the curvature effect of the dendritic tip during the solidification, and the curvature effect leads to the solid line descending; nevertheless, the diffusivity of the solute in solid is far less than the velocity of the dendritic tip growth[9]. The concentration in the front interface of undercooled melting enriches, due to the solute redistribution during the course of solidification, which makes the concentration of solid phase be lower than the initial concentration, and the speed of the solute diffusivity in liquid phase be less than that of the dendritic growth, so that the solute educed from the solid during solidifying can't spread to the liquid fully.

Due to the rapidest growth speed of dendritic tip, the solute doesn't diffuse timely, the solute gradients of the tip is the highest. Furthermore, in the mushy regions between the dendritic secondary arms, the solute isn't easy to diffuse, leading to the concentration is the highest.

From Fig.1(b), it can also be found that, on the bottom of the primary arm's, the fracture appears in parts of the sidebranches' roots, this can be explained as follows: when the dendritic grows to certain extent, and the computation domain is limited, which make the solute unable to diffuse adequately, leading to the higher solute supersaturation, as a result, the dendritic fracture happens[10]. Coalescence occurs between some side-branches.

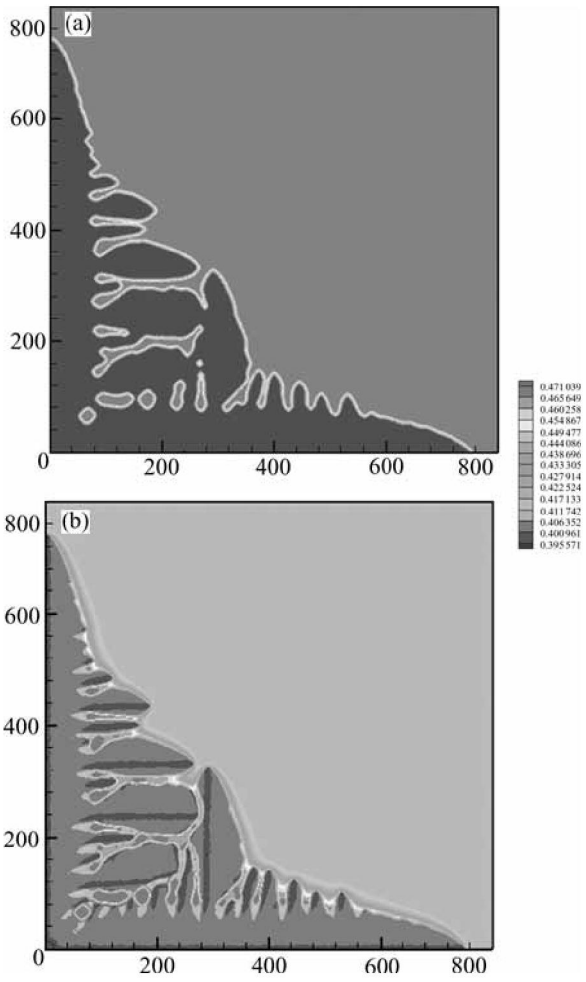


**Fig.1** Dendrite pattern and concentration field: (a) Dendritic pattern; (b) Concentration field

Fig.2 shows the solute profile in the front interface and the phase-field profile when the main branches' dendritic tip traverses through the solid/liquid interface along with $X$ axis at a growth time of $5.5\times10^{-4}$ s. From

the figure, it can be found that the solute profile of solid phase region appears to fluctuation, because the mathematical model used in this paper neglects the influence of solute gradient term on the solute distribution, which makes the interface moving velocity fluctuate acutely with the growth time, inducing the solute partition coefficient $k$ in the front interface to fluctuate accordingly, in the end, leading to the solute profile of solid phase region fluctuate[11]. It can be found that there is a diffusion layer in the liquid phase region in the front interface, and in the diffusion layer, the solute concentration presents the index relation and decays along the direction of the initial composition. In a certain distance behind the front interface the concentration value equals the initial concentration again, due to the re-distribution of solution in liquid phase by diffusion. Otherwise, it can be seen that an area increases sharply in solute profile appearing in the solid/liquid interface region, the area holding the length of 6 grids is the value of interfacial thickness.

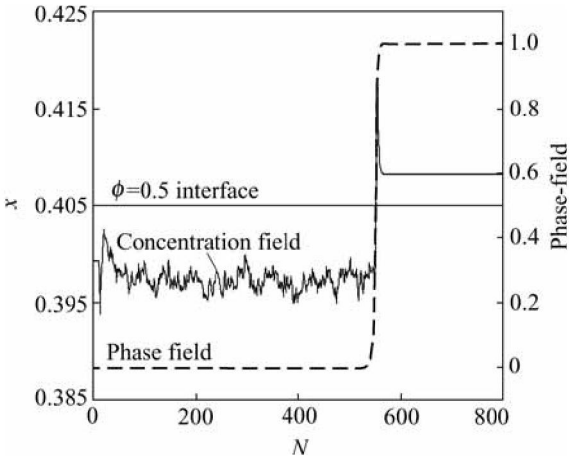


**Fig.2** Solute profile in front interface and phase-field profile at growth time of $5.5\times10^{-4}$ s with $\gamma$=0.05

### 3.2 Effect of noise amplitude $\alpha$ on microsegregation patterns

The influence of noise amplitude $\alpha$ on the simulation results is obvious. Fig.3 shows the main branches' solute profiles along with $X$ axis under different $\alpha$ at the growth time $9.0\times10^{-5}$ s with $\gamma$=0.05, other material parameters are selected, as listed in Table 1. It can be found that, without noise ($\alpha$=0), no fluctuation appears to solute composition in the solid, and the growth velocity is relatively high. But with noise ($\alpha>0$), the solute composition in the solid begins to fluctuate. If an appropriate level of noise amplitude is assigned to $\alpha$, with the increment of $\alpha$, the dendritic tip velocity and the tip radius don't change, the fluctuant scope of solute composition in the solid is steady, which indicates that, when an appropriate value is assigned to $\alpha$, noise can enhances the emergence of the sidebranch but not influences the dendritic tip operating state. When $\alpha$ gets bigger, the solute composition in the solid fluctuate acutely, and the dendritic tip velocity reduces accordingly, which indicates that the steady state of dendritic tip is disturbed. From Fig.3, it also can be seen that, with the increment of $\alpha$, the solid/liquid interface corresponding to the peak value of concentration rises, while the lowest value of the solid concentration falls accordingly, as a result, the microsegregation in the front interfere aggravates, therefore, the value of $\alpha$ must be tried again and again.

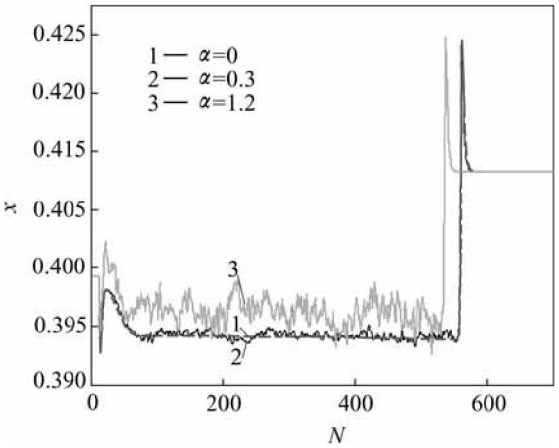


**Fig.3** Solute profile along with growth direction under different $\alpha$ at growth time $9.0\times10^{-5}$ s with $\gamma$=0.05

### 3.3 Effect of interface kinetic coefficient $\beta$ on microsegregation patterns

The influence of interface kinetic coefficient($\beta$) on dendritic growth is reflected by Gibbs-Thompson formula, representing the growth interface's offset from balance. The selection of $\beta$ is vital in the simulation. And although $\beta$ relates to the growth velocity and the interfacial undercooling, the effect of the interface kinetic coefficient on dendritic growth is complicated.

Fig.4 presents the main branches' solute profiles along with $X$ axis under different $\beta$ at growth time $6.0\times10^{-5}$ s with $\gamma$=0.05. From the figure, it can be found that, with the increment of $\beta$, the dendritic tip growth velocity rises accordingly, and also the solute composition in the solid fluctuates acutely, because the fluctuation of the solute partition coefficient $k$ falls with the growth velocity decreasing, therefore, the fluctuation of the solute composition in the solid reduces accordingly. It also can be found that, with the increment of $\beta$, the solute diffusion layer in the front solid/liquid interface is thinner, due to the diffusion layer baffles the release of the solute to liquid, so the bigger $\beta$, the smaller the resistance of the diffusion layer to the solute diffusion to liquid, and the more developed the sidebranching. With the increment of $\beta$, the solid/liquid interface corresponding to the peak value of concentration falls, while

the lowest value of the solid concentration rises accordingly, as a result, the microsegregation in the front interface alleviates, due to the increment of growth velocity, the solid composition $x_s$ and the liquid composition $x_l$ approach, consequently, presenting the solute trapping.

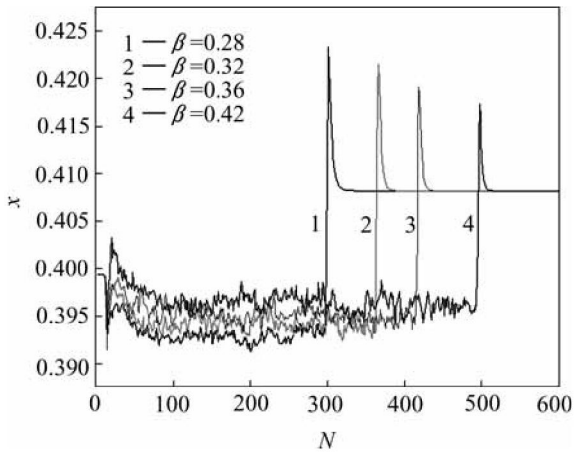


**Fig.4** Solute profile along with growth direction under different $\beta$ at growth time $6.0\times10^{-5}$ s with $\gamma$=0.05

### 3.4 Effect of anisotropy parameter $\gamma$ on microsegregation patterns

The anisotropy parameter $\gamma$ represents the anisotropic intension of surface energy, interface thickness and kinetics. It is not clear how to set the value of the anisotropy coefficient exactly and what its connection with real physical parameters is[12]. However, The anisotropy parameter $\gamma$ is so important to the dendritic growth that it cannot be ignored. The main branches' solute profiles along with $X$ axis under different $\gamma$ at the growth time $6.0\times10^{-5}$ s are shown in Fig.5. From the figure, it can be seen that, with the increment of $\gamma$, the solute diffusion layer in the front solid/liquid interface becomes thicker; both the main branches and sidebranch become slender, and the DAS(Secondary Dendrite Arm Spacing) becomes smaller, while the dendritic tip growth velocity rises accordingly, the solute composition in the solid fluctuates acutely, and the severity of microsegregation aggravates. Because the increased level of $\gamma$ makes the noise be amplified quickly, the surface energy cannot restrain effectively the amplification, and then the interface becomes unstable, which causes the sidebranch to split constantly.

### 3.5 Effect of surface energy($\sigma$) on microsegregation patterns

The interface has great effect, and sometimes crucial effect, on the material performance. The interfacial structure and interfacial behavior are related to surface energy $\sigma$. Surface energy $\sigma$ is one of the important cause affecting the dendritic growth. Fig.6 shows the main branches' solute profiles along with $X$ axis under different $\sigma$ at the growth time of $6.0\times10^{-5}$ s with $\gamma$=0.05. From the figure, it can be found that, with the increment of $\sigma$, the dendritic tip velocity rises accordingly, but the fluctuation of the solute composition in the solid reduces accordingly, because the increment of surface energy $\sigma$ is in favor of solid/liquid interfacial stabilization, and makes the noise be difficult to be amplified. The increased level of the surface energy $\sigma$ increases with the inducement time, and decrease the nucleation velocity, as a result, increases the dendritic size, contrarily, refine the grain. With the decrement of $\sigma$, the dendritic growth velocity reduces, thereby, the dendritic growth is restrained effectively. At the same time, with the increment of $\sigma$, the solid/liquid interface corresponding to the peak value of concentration falls, while the lowest value of the solid concentration rises accordingly, consequently, the microsegregation in the front interfere reduces, because the increment of growth velocity, the solid composition $x_s$ and the liquid composition $x_l$ approach, as a result, presenting the solute trapping.

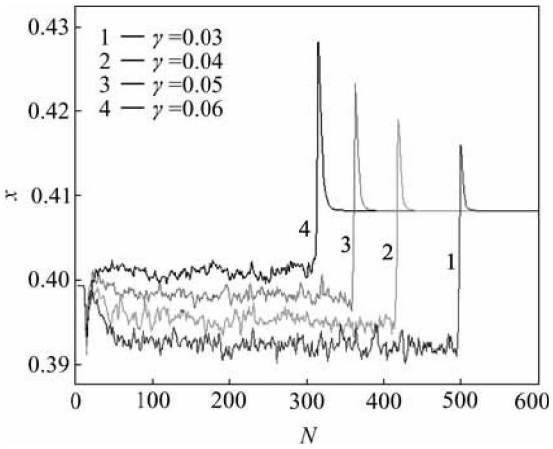


**Fig.5** Solute profile along with growth direction under different $\gamma$ at growth time $t$=$6.0\times10^{-5}$ s

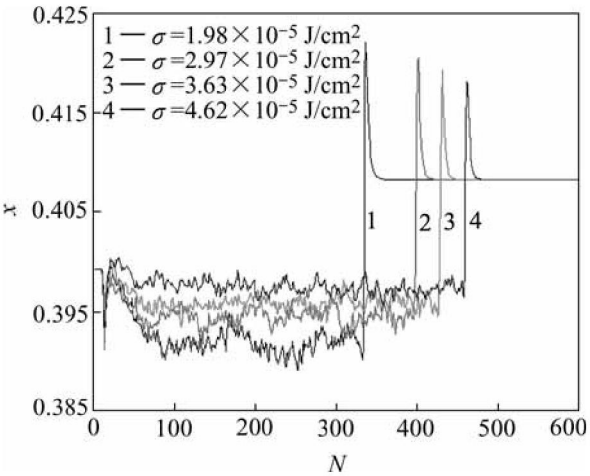


**Fig.6** Solute profile along with growth direction under different $\sigma$ at growth time of $6.0\times10^{-5}$ s with $\gamma$=0.05

## 4 Conclusions

1) In the phase-field simulations of micro-segregation, different noise amplitude $\alpha$ ,interface kinetic coefficient $\beta$, anisotropy parameter $\gamma$ and surface energy $\sigma$ lead to different severity of microsegregation.

2) The larger the interface kinetic coefficient $\beta$, the more acutely the solute composition in the solid fluctuates, but the severity of microsegregation in the front interface reduces.

3) At larger surface energy $\sigma$, the fluctuant scope of solute composition in the solid is smaller, and the degree of microsegregation is smaller.

4) With the increment of anisotropy parameter $\gamma$, the fluctuation of solute composition in the solid becomes more acutely, and the severity of microsegregation in the front interface aggravates.

5) When an appropriate value is assigned to $\sigma$, the fluctuant scope of solute composition in the solid is steady, and the influence of $\alpha$ on microsegregation is small.

## References

[1] KARMA A, RAPPEL W J. Phase-field model of dendritic side-branching with thermal noise [J]. Phys Rev E, 1999, 60(4): 3164–3624.

[2] KIM J H, J W PARK, LEE C H, et al. Numerical modeling of micro-segregation in binary alloys [J]. Journal of Crystal Growth, 1997, 173: 550–560.

[3] KOBAYASHI R. Modeling and numerical simulation of dendritic crystal growth [J]. Journal of Computation Physics, 1999, 154(1): 410–415.

[4] MURRAY B T, WHEELER A A, GLICKSMAN M E. Simulation of experimentally observed dendritic growth behavior using phase-field model [J]. J Cryst Growth, 1995, 154: 386–400.

[5] KARMA A, RAPPEL W J. Phase field method for computationally efficient modeling of solidification with arbitrary interface kinetics [J]. Phys Rev E, 1996, 53(4): R3017.

[6] ZHU Chang-sheng, WANG Zhi-ping, LIU Bai-cheng, et al. Effects of phase-field parameters of sidebranching using phase field simulation [J]. Chinese Journal of Mechanical Engineering, 2005, 41: 30–34.

[7] CONTI M. Solidification of binary alloys: Thermal effects studied with the phase field model [J]. Phys Rev E, 1997, 55(1): 765–771.

[8] WARREN J A, BOETTINGER W J. Prediction of dendritic growth and microsegregation patterns in a binary alloy using the phase-field method [J]. Acta Mater, 1994, 43(2): 689–703.

[9] LONG Wen-yuan, CAI Qi-zhou, CHEN Li-liang, et al. Phase-field simulations of solidification of Al-Cu binary alloys [J]. Trans Nonferrous Met Soc China, 2004, 14: 291–296.

[10] YU Yan-mei, YANG Gen-cang, ZHAO Da-wen, et al. Effects of temperature boundary conditions on equiaxed dendritic growth in phase-field simulations of binary alloy [J]. Trans Nonferrous Met Soc China, 2002, 12(6): 1064–1068.

[11] LI Mei-e, YANG Gen-cang, ZHOU Yao-he. Phase-field modeling of directional solidification of a binary alloy at high velocities [J]. Acta Phys Sin, 2005, 54: 454–459.

[12] ZHU Chang-sheng, WANG Zhi-ping, JING Tao. Phase-field simulation of dendritic sidebranching induced by thermal noise [J]. Trans Nonferrous Met Soc China, 2004, 12(6): 1106–1110.

**(Edited by LI Xiang-qun)**